

# PAD3R: Pose-Aware Dynamic 3D Reconstruction from Casual Videos

TING-HSUAN LIAO\*, University of Maryland College Park, USA

HAOWEN LIU\*, University of Maryland College Park, USA

YIRAN XU, University of Maryland College Park, USA

SONGWEI GE, University of Maryland College Park, USA

GENGSHAN YANG†

JIA-BIN HUANG†, University of Maryland College Park, USA



**Fig. 1. Complete 3D reconstruction of dynamic objects from a single unposed video.** Given a casually captured monocular video (left), our method reconstructs accurate object-centric camera poses, high-quality geometry, appearance, and non-rigid deformations over time (right). Leveraging the capabilities of generative models and differentiable rendering, PAD3R recovers complete, plausible 3D shape and deformations, remaining robust to significant root body, camera movement, and limited viewpoints. Images sourced from DAVIS (©DAVIS Challenge organizers) and ©Pexels.

We present PAD3R, a method for reconstructing deformable 3D objects from casually captured, unposed monocular videos. Unlike existing approaches,

\*Co-first authors.

†Joint advising.

Authors' Contact Information: Ting-Hsuan Liao, University of Maryland College Park, USA., ting129@umd.edu; Haowen Liu, University of Maryland College Park, USA., hwl@umd.edu; Yiran Xu, University of Maryland College Park, USA., yiranx@umd.edu; Songwei Ge, University of Maryland College Park, USA., songweig@umd.edu; Gengshan Yang, y.gengshan@gmail.com; Jia-Bin Huang, University of Maryland College Park, USA., jbhuang@umd.edu.

Permission to make digital or hard copies of all or part of this work for personal or classroom use is granted without fee provided that copies are not made or distributed for profit or commercial advantage and that copies bear this notice and the full citation on the first page. Copyrights for components of this work owned by others than the author(s) must be honored. Abstracting with credit is permitted. To copy otherwise, or republish, to post on servers or to redistribute to lists, requires prior specific permission and/or a fee. Request permissions from permissions@acm.org.

PAD3R handles long video sequences that feature substantial object deformation, large-scale camera movement, and limited view coverage, which typically challenge conventional systems. At its core, our approach trains a personalized, object-centric pose estimator, supervised by a pre-trained image-to-3D model. This guides the optimization of deformable 3D Gaussian representation. The optimization is further regularized by long-term 2D point tracking over the entire input video. By combining generative priors and differentiable rendering, PAD3R reconstructs high-fidelity, articulated 3D representations of objects in a category-agnostic way. Extensive qualitative and quantitative results show that PAD3R is robust and generalizes well across challenging scenarios, highlighting its potential for dynamic scene understanding and 3D content creation. Please refer to our project page for more details: [PAD3R.github.io](https://PAD3R.github.io).

© 2025 Copyright held by the owner/author(s). Publication rights licensed to ACM. ACM 1557-7368/2025/9-ART  
<https://doi.org/10.1145/nnnnnnnnnnnnnn>

CCS Concepts: • Computing methodologies → Animation; Shape modeling; Rendering; Computer vision.

Additional Key Words and Phrases: 4D reconstruction and generation, animal reconstruction and tracking, novel view synthesis

**ACM Reference Format:**

Ting-Hsuan Liao, Haowen Liu, Yiran Xu, Songwei Ge, Gengshan Yang, and Jia-Bin Huang. 2025. PAD3R: Pose-Aware Dynamic 3D Reconstruction from Casual Videos. *ACM Trans. Graph.* 1, 1 (September 2025), 11 pages. <https://doi.org/10.1145/nmmnnnn.nmmnnnn>

## 1 Introduction

Reconstructing dynamic 3D objects from monocular videos is crucial for applications in gaming, film production, augmented and virtual reality, and robotics [Yunus et al. 2024]. However, this task remains challenging due to its ill-posed nature, where infinitely many 3D interpretations explain the same 2D observations. Classic approaches often rely heavily on specialized sensors [Park and Hodgins 2006] or category-specific models [Loper et al. 2015], limiting their applicability to diverse objects and scenes in real-world environments.

Recent advances in differentiable rendering techniques such as Neural Radiance Fields (NeRF) and 3D Gaussian Splatting, along with their dynamic extensions [Luiten et al. 2024; Park et al. 2021a,b; Pumarola et al. 2021; Song et al. 2023; Wu et al. 2024], have significantly improved 3D/4D reconstructions of general scenes. However, these approaches often require precise camera poses and dense viewpoint coverage. To overcome this dependency, a line of work [Jiang et al. 2024; Li et al. 2024; Ren et al. 2023; Tu et al. 2025; Zeng et al. 2024; Zhang et al. 2024] incorporates generative priors from pre-trained 2D (or multi-view) diffusion models into 4D reconstruction pipelines using Score Distillation Sampling (SDS) and its variants. But such approaches are limited to videos from a static viewpoint in a synthetic setup. Several recent methods [Ren et al. 2024; Wu et al. 2025; Xie et al. 2024] finetune video diffusion models for inferring the multi-view views of dynamic 3D objects directly from monocular videos. Nonetheless, their effectiveness hinges on high-quality multi-view training data, limiting generalization to complex, out-of-distribution real-world videos, many of which involve large camera and object motion unseen during training. Hence, robust dynamic 3D reconstruction from in-the-wild monocular videos remains an open challenge.

In this paper, we introduce PAD3R, a method that tackles the challenge of learning a deformable 3D representation of a target object from a single casually captured unposed video. Our core idea is to leverage both the generative diffusion prior (for recovering a static 3D representation) and differentiable rendering (for jointly estimating object-centric camera poses and time-varying deformation). Given a video, we first use an image-to-3D method [Liu et al. 2023] to obtain a static canonical 3D model from a keyframe. We then train a *personalized* object-centric camera pose estimator, by fine-tuning DINO-v2 [Oquab et al. 2023], using renderings of the generated 3D model sampled from random viewpoints. This pose initialization is critical for the subsequent dynamic reconstruction stage. We initialize a hybrid 3D Gaussian representation using the canonical geometry and predicted poses. Optimizing the temporal

deformation model solely using photometric reconstruction loss is difficult due to large object deformation, self-occlusion, and limited view coverage. We regularize the training with motion cues from a persistent point tracker [Karaev et al. 2024], augmented with a proposed multi-chunk strategy aggregating occluded signals across frames. We validate the proposed method through extensive experiments on diverse real and synthetic video datasets. Our approach consistently outperforms state-of-the-art methods in both qualitative and quantitative evaluations. Ablation studies further validate the importance of our design choices in improving reconstruction accuracy and temporal coherence.

Our contributions are as follows.

- We leverage an image-to-3D model to learn object-centric camera poses, providing crucial initialization for the subsequent 4D reconstruction stage.
- We introduce a multi-chunk strategy that effectively uses long-term motion cues from 2d point tracking to regularize object deformation.
- We evaluate our method on both synthetic datasets, including Consistent4D and Artemis, as well as challenging real-world videos. PAD3R demonstrates state-of-the art 4D reconstruction results and robustness to real world camera motion. We will release our code to support and foster future research.

## 2 Related Work

**Dynamic Scene Reconstruction.** Dynamic scene reconstruction aims to recover a dynamic 3D scene from videos, supporting both viewpoint- and time-varying rendering. Building on the success of Neural Radiance Fields (NeRFs) [Mildenhall et al. 2020], several works [Gao et al. 2021; Park et al. 2021a,b; Pumarola et al. 2021] have extended NeRFs to dynamic settings. However, due to the volumetric rendering nature of these methods, they often require time-consuming optimization, even with efficiency-focused advancements [Cao and Johnson 2023; Fridovich-Keil et al. 2023]. Recently, 3D Gaussian Splatting (3DGS) [Kerbl et al. 2023] introduces a significantly faster rendering pipeline, making high-quality, real-time dynamic scene rendering possible. A series of work [Duan et al. 2024; Luiten et al. 2024; Wu et al. 2024; Yang et al. 2024, 2023] extend 3DGS by introducing an additional deformation field. However, these methods struggle to model complex non-rigid deformations or sparse views. Although regularization [Guédon and Lepetit 2024; Lei et al. 2024; Wang et al. 2024; Yang et al. 2022] is employed, they still struggle with reconstructing a monocular video, resulting in suboptimal results. More recent works [Lei et al. 2024; Liu et al. 2025; Stearns et al. 2024; Wang et al. 2024, 2025b] tackle reconstruction from a single monocular video, but primarily focus on scenes. These methods demonstrate limited view ranges in novel view rendering. In contrast, our method focuses on *full 360° reconstruction* of dynamic 3D objects with complex deformations from a single monocular video.

**4D Reconstruction with Generative Priors.** Inspired by the success of generative modeling [Ho et al. 2020; Song et al. 2021], recent works [Jiang et al. 2024; Li et al. 2024; Pan et al. 2024; Ren et al. 2023; Tu et al. 2025; Wang et al. 2023b; Yin et al. 2023; Zeng et al. 2024;

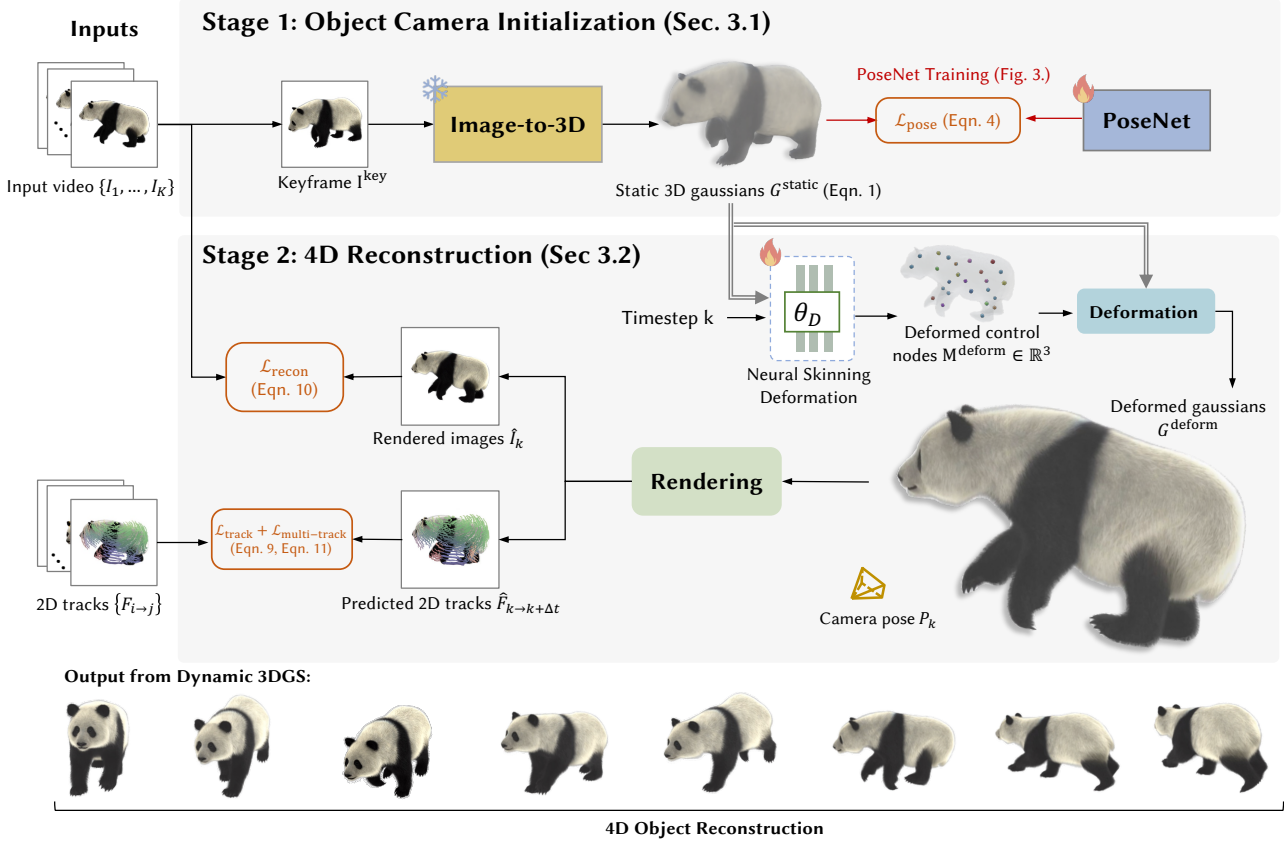


Fig. 2. **Method overview.** Our method consists of two main stages. In the first stage, we select a frame from the video sequence as the canonical frame (or keyframe), and use an image-to-3D model [Liu et al. 2023] to obtain a static 3D Gaussian  $\hat{G}$ . We then render  $\hat{G}$  from a set of randomly sampled camera poses to fine-tune a lightweight image-to-pose estimator, PoseNet, using DINO-v2 backbone. The full training scheme is illustrated in Figure. 3. Then, we use the camera pose estimator to initialize the camera pose of every input video frame and optimize a deformable 3D object model. Images sourced from Artemis (©Luo et al., 2022).

Zhang et al. 2024; Zhao et al. 2023] have explored incorporating generative priors into 4D reconstruction pipelines to reduce reliance on densely-captured multi-view data. Score Distillation Sampling (SDS) and its variants [Poole et al. 2023; Wang et al. 2023a; Yi et al. 2024] are commonly adopted to supervise reconstruction from unseen views. However, these methods typically assume fixed camera poses and root-body object motions, severely limiting their applicability to real-world videos with complex camera trajectories and dynamic object motion. In contrast, we propose a more robust approach to handle such challenging scenarios.

**4D Reconstruction with Feed-Forward Models.** Recent methods [Park et al. 2025; Ren et al. 2024; Wu et al. 2025; Xie et al. 2024] directly train video diffusion or feed-forward models for spatio-temporally consistent 4D generation from a monocular video, without relying on test-time optimization. However, their performance heavily depends on the quality and diversity of multi-view video data used during training. As a result, these methods often struggle to generalize to out-of-distribution real-world videos, particularly those with complex object and camera motions not seen in the training datasets [Deitke et al. 2023; Ren et al. 2024; Wu et al. 2025; Xie

et al. 2024]. In this paper, we introduce a robust method, PAD3R, for addressing such challenges and demonstrate superior performance over feed-forward baselines.

### 3 Method

Given a monocular video sequence  $\{I_1, I_2, \dots, I_K\}$  containing  $K$  RGB images that depict a dynamic, articulated object (such as a person or animal), our objective is to reconstruct its complete time-varying 3D geometry. This task is inherently ill-posed and we solve it in two stages: 1) camera pose initialization and 2) dynamic Gaussian splatting reconstruction. An overview of our approach is in Figure 2.

#### 3.1 Object-centric Camera Pose Initialization

A key ambiguity in dynamic 3D reconstruction from in-the-wild videos comes from the entanglement of camera and object motions. As we focus on reconstructing the *dynamic object*, we need to explicitly model the camera poses with respect to the dynamic object (not to the scene). Note that this is a more challenging case than

estimating camera poses with respect to the static scene due to the lack of rigidity constraints.

Instead of solving both camera and object motions simultaneously through optimization, we first estimate the camera pose of each input frame, *relative to the object's coordinate system*. These estimates serve as initialization for the subsequent joint optimization stage. While our method targets non-rigid objects, we assume their overall shape and appearance remain relatively consistent throughout the video. This assumption enables reliable pose estimation by training a personalized pose prediction model for each object instance, using only a single-frame 3D reconstruction as supervision, illustrated in Figure 3.

We begin by selecting a keyframe  $I^{\text{key}}$  from the video and generating a 3D representation conditioned on this image. The keyframe is selected such that the object appears in a common, well-posed configuration (e.g., the side view of a standing animal), which helps avoid inaccuracies in generation due to extreme or unusual poses.

To overcome the geometric limitations of naive 3DGs in geometric modeling, we adopt SuGaR [Guédon and Lepetit 2024], a hybrid Gaussian representation. SuGaR enhances surface modeling by introducing a regularization term that aligns Gaussians with mesh surfaces, enabling more accurate geometry and mesh-based operations such as deformation.

We denote the SuGaR model as  $G^{\text{static}} = \{\mathcal{V}, \mathcal{F}, \hat{G}\}$ , where  $\mathcal{V}$  and  $\mathcal{F}$  are the mesh vertices and faces, respectively, and  $\hat{G}$  is the set of 3D Gaussians anchored to mesh surfaces. Each face  $f \in \mathcal{F}$  is associated with a fixed number of Gaussians, whose positions are parameterized using barycentric coordinates. The resulting set of Gaussians  $\hat{G}$  is defined as:

$$\hat{G} = \{\mu_i, \Sigma_i, c_i, \alpha_i\}_{i=1}^N, \quad (1)$$

where  $\mu_i$  is the mean,  $\Sigma_i$  is a positive semi-definite covariance matrix,  $c_i$  is the view-dependent color parametrized using spherical harmonics (SH), and  $\alpha_i$  is the opacity value.

Following the approach in [Li et al. 2024], we begin by generating a coarse mesh using an off-the-shelf image-to-3D method [Liu et al. 2023]. To enrich surface detail, we attach six flat Gaussians to each triangle face of the mesh. We then optimize the SuGaR model with photometric reconstruction loss  $\mathcal{L}_{\text{photo}}$  on the reference view and Score Distillation Sampling (SDS) loss on unseen views:

$$\mathcal{L}_{\text{3D}} = \lambda_{\text{photo}} \mathcal{L}_{\text{photo}} + \lambda_{\text{sds}} \mathcal{L}_{\text{sds}}, \quad (2)$$

where

$$\mathcal{L}_{\text{sds}} = \mathbb{E}_{\mathbf{x} \sim \mathcal{N}(0, I), t \sim \mathcal{U}(0, T)} \left[ w(t) \|\epsilon_{\theta}(\mathbf{x}_t, t) - \epsilon\|_2^2 \right]. \quad (3)$$

Here,  $\mathbf{x}_t$  denotes the noisy latent at timestep  $t$ ,  $\epsilon_{\theta}$  is the predicted noise from the score network,  $\epsilon$  is the ground truth noise, and  $w(t)$  is a time-dependent weighting function.

Using the optimized Gaussian model—though any other 3D representation could be used—we synthesize images  $C_l$  by rendering with randomly sampled camera poses  $\pi_l = (\mathbf{R}_l, \mathbf{T}_l)$ . We train the pose estimation model  $E$  on these rendered images, augmented with color jitter, random masking, and rotations. The pose estimation model  $E$  uses a pre-trained DINOv2 [Oquab et al. 2023] backbone with a multi-layer perceptron (MLP) regression head to predict the

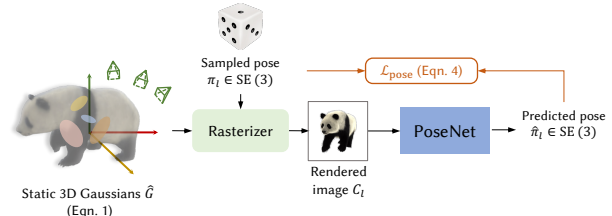


Fig. 3. **Training personalized PoseNet.** To train the pose estimator network  $E$ , we first obtain a static Gaussian model of the selected canonical frame  $I^{\text{key}}$ . At each training iteration, we render images  $C_l$  on-the-fly from the model with randomly sampled camera poses. These images are used to train the network to predict 6-DoF camera poses, parameterized by translations and quaternion rotations.

6-DoF camera pose in the object coordinate system, by minimizing the pose loss  $\mathcal{L}_{\text{pose}}$ :

$$\mathcal{L}_{\text{pose}} = \lambda_{\text{rot}} \mathcal{L}_{\text{rot}} + \lambda_{\text{trans}} \mathcal{L}_{\text{trans}} + \lambda_{\text{unc}} \mathcal{L}_{\text{unc}}, \quad (4)$$

where  $\mathcal{L}_{\text{trans}}$  and  $\mathcal{L}_{\text{rot}}$  denote the translational and rotational components respectively:

$$\mathcal{L}_{\text{trans}} = \|\mathbf{T} - \hat{\mathbf{T}}\|_2^2, \quad \mathcal{L}_{\text{rot}} = \arccos((\text{Tr}(\mathbf{R}\hat{\mathbf{R}}^T) - 1)/2), \quad (5)$$

where  $\pi = (\mathbf{R}, \mathbf{T})$  denotes the ground-truth camera pose consisting of rotation  $\mathbf{R}$  and translation  $\mathbf{T}$ , and  $\hat{\pi} = (\hat{\mathbf{R}}, \hat{\mathbf{T}})$  is the predicted poses from the network. In addition, we incorporate an uncertainty loss  $\mathcal{L}_{\text{unc}}$  to account for the confidence of the pose predictions [Kendall and Gal 2017], encouraging the predicted uncertainty  $\sigma$  to reflect the actual pose error magnitude:

$$\mathcal{L}_{\text{unc}} = (\sigma - (\mathcal{L}_{\text{rot}} + \mathcal{L}_{\text{trans}}))^2, \quad (6)$$

Using the trained pose estimator, we initialize the camera pose  $P_k$  for each input frame  $I_k$  in the video sequence as initialization for subsequent optimizations.

### 3.2 Dynamic Gaussian Splats Reconstruction

**Neural Skinning Deformation Model** To model dynamic motion, we uniformly sample a set of control nodes  $M$  anchored to mesh vertices in the static SuGaR model  $G^{\text{static}}$ . The deformation model  $\theta_D$ , conditioned on the video timestep  $k$ , predicts per-frame deformations of these nodes.

We adopt the hybrid deformation framework from [Li et al. 2024], where each vertex deformation is computed by blending transformations from neighboring control nodes using a combination of Linear Blend Skinning (LBS) [Sumner et al. 2007] and Dual Quaternion Skinning (DQS) [Kavan et al. 2008]. Each control node carries rotation, shear, and translation, and a learned rigidity score that modulates its influence. The final deformation at each vertex is computed by interpolating between LBS and DQS results, weighted by the aggregated local rigidity from neighboring nodes.

**Dense tracking supervision** While photometric losses can provide appearance-based supervision from input frames, but they offer limited guidance on dynamic object motion. To address this,

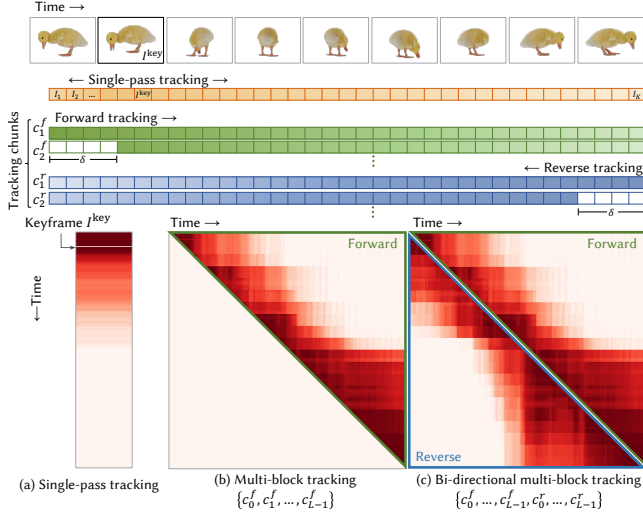


**Fig. 4. Co-visibility of tracked points across time.** Given a video sequence  $\{I_1, I_2, \dots, I_K\}$ , we extract dense correspondences using a 2D tracking model [Karaev et al. 2024]. Each colored block represents the frame range tracked from a specific starting frame, with a temporal stride of  $\delta = 4$  in this illustration. (a) **Single-pass tracking starting from the canonical frame  $I^{\text{key}}$**  provides strong guidance in the canonical space but has limited coverage in distant frames due to occlusion or narrow field of view. (b) **Multi-block tracking** (we show forward tracking  $\{c_0^f, c_1^f, \dots, c_{L-1}^f\}$  here) improves coverage by dividing the video into chunks and tracking forward only, but lacks symmetric temporal consistency. (c) **Our proposed bi-directional multi-block tracking** strategy combines forward  $\{c_i^f\}$  and reverse  $\{c_i^r\}$  tracking across overlapping chunks, yielding dense, bidirectional correspondences between all frame pairs. Images sourced from Artemis (©Luo et al., 2022).

we incorporate dense 2D tracking [Karaev et al. 2024] which captures temporal correspondences and motion dynamics in image space. This enables spatially and temporally coherent supervision for 4D reconstruction from monocular video. Given a sequence of  $K$  frames, the tracker predicts a set of tracked 2D points across the sequence, including pixel locations and visibility masks. We denote the tracked 2D coordinates as  $x_k^d \in \mathbb{R}^2$  and visibility as  $v_k^d \in \{0, 1\}$ , where  $k \in [0, K)$  and  $d \in [0, D)$  indexes tracked points.

To supervise the canonical 3D model over time, we construct single-pass point trajectories anchored at the selected keyframe. Starting from the selected keyframe  $I^{\text{key}}$ , we run the tracker in both forward ( $I^{\text{key}} \rightarrow K$ ) and backward ( $I^{\text{key}} \rightarrow 0$ ) through the video, resulting in long-range, temporally consistent trajectories aligned with the canonical view.

Using the reconstructed 3D mesh at the keyframe  $I^{\text{key}}$ , we lift each 2D point  $x_k^d$  into a 3D point  $X^d \in \mathbb{R}^3$  on the surface via ray-mesh intersection. These 3D anchors establish correspondence between 2D tracks and the canonical 3D space.

However, a single frame can only cover a small field of view, leaving many pixels in the distant frames to be untracked. To address this, we apply bi-directional multi-block tracking by partitioning

the video into  $L$  overlapping chunks to increase track density and supervision coverage:

$$\text{forward: } [k_0 : K], [k_1 : K], \dots, [k_{L-1} : K] \quad (7)$$

$$\text{reverse: } [K - k_0 : 0], [K - k_1 : 0], \dots, [K - k_{L-1} : 0], \quad (8)$$

where  $k_i = i \cdot \delta$ , for  $k = 0, 1, \dots, L - 1$ , and  $\delta$  is the temporal stride.

Each chunk tracks points from its start frame  $k_i$  to the end of the video, ensuring that for any frame pair  $(i, j)$ , at least one chunk covers both frames. To select the optimal chunk for each pair  $(i, j)$ , we evaluate the number of commonly visible tracks across all chunks and chose the one with the highest overlap. We illustrate the proposed sampling strategy in Figure 4.

For each tracked point  $x_{\text{key}}^d$  with the known 3D position  $X^d$  from single-pass tracking, we find the corresponding Gaussian splatting points  $g^d$  in the canonical model via nearest-neighbor search in 3D. At each timestep  $k$ , we project these Gaussian points  $g^d$  to obtain the predicted 2D location  $\hat{x}_k^d$ . We compute a tracking loss as

$$\mathcal{L}_{\text{track}} = \sum_{k, d} v_k^d \cdot |\hat{x}_k^d - x_k^d| \quad (9)$$

where  $v_k^d$  is a visibility mask that excludes the invisible points.

For bi-directional multi-block tracking, we compute the 2D tracks between any two frames  $(i, j)$  as:

$$\mathbf{F}_{i \rightarrow j}^d = x_j^d - x_i^d, \quad (10)$$

where  $d \in \mathcal{D}_{i, j}$  is visible in both frames  $i$  and  $j$ .

For every two frames, we compute its motion in 3D space across frames and project it to 2D track  $\hat{\mathbf{F}}_{i, j}^d$  via rasterization. This prediction is supervised against the tracked flow with a masked L2 loss:

$$\mathcal{L}_{\text{multi-track}} = \sum_{i < j, d} m_{i, j}^d \cdot \|\hat{\mathbf{F}}_{i \rightarrow j}^d - \mathbf{F}_{i \rightarrow j}^d\|_2^2, \quad (11)$$

where  $m_{i, j}^d$  indicates visibility of point  $d$  in both frames.

This dual strategy delivers robust, spatially dense supervision, enabling accurate and consistent reconstruction of dynamic geometry even under challenging visibility and motion conditions.

**Optimization** The overall objective in the reference view reconstruction stage combines several losses. In addition to a photometric loss that supervises appearance consistency, we apply an as-rigid-as-possible (ARAP) regularization term [Sorkine and Alexa 2007] to promote locally consistent deformation of the hybrid Gaussian surface.

The ARAP loss penalizes deviations from locally rigid transformations between neighboring vertex pairs and is defined as:

$$\mathcal{L}_{\text{ARAP}} = \sum_{\mathbf{v} \in \mathcal{V}} \sum_{\mathbf{v}_n \in \mathcal{N}(\mathbf{v})} \omega_n(\mathbf{v}) \|(\tilde{\mathbf{v}} - \tilde{\mathbf{v}}_n) - R_{\mathbf{v}}(\mathbf{v} - \mathbf{v}_n)\|_2^2. \quad (12)$$

Here,  $\mathcal{V}$  is the set of mesh vertices,  $\mathcal{N}(\mathbf{v})$  denotes the 1-ring neighbors of vertex  $\mathbf{v}$ . The variables  $\omega_n(\mathbf{v})$  is the cotangent weight associated with neighbor  $\mathbf{v}_n$ . The variables  $\tilde{\mathbf{v}}$  and  $\tilde{\mathbf{v}}_n$  represent deformed vertex positions, and  $R_{\mathbf{v}}$  is the locally estimated rotation at vertex  $\mathbf{v}$ .

The full loss jointly optimizes both the deformation network and the pose network and is formulated as:

$$\mathcal{L}_{\text{4D}} = \lambda_{\text{rgb}} \mathcal{L}_{\text{rgb}} + \lambda_{\text{track}} \mathcal{L}_{\text{track}} + \lambda_{\text{multi}} \mathcal{L}_{\text{multi-track}} + \lambda_{\text{arap}} \mathcal{L}_{\text{ARAP}}, \quad (13)$$

where each weight  $\lambda$  controls the contributions of its corresponding term. The photometric loss  $\mathcal{L}_{\text{rgb}} = \|\hat{I} - I\|_2^2$  measures the mean squared error between the rendered image  $\hat{I}$  and the ground truth input frame  $I$ . Additionally, we optimize a per-frame delta camera pose parameterized by an MLP simultaneously.

## 4 Experiments

### 4.1 Dataset

We quantitatively evaluate PAD3R on the Consistent4D [Jiang et al. 2024] dataset, which includes seven multi-view videos, each with 32 frames. For each sequence, a single-view video is used as input, while the remaining four views serve as evaluation references. Since Consistent4D features *static* cameras only, we introduce a new benchmark based on the Artemis dataset [Luo et al. 2022]. The dataset contains multi-view videos of animals with varying camera motion and viewpoint coverage. To create this benchmark, we sample camera views that collectively span a target angular range around the animal, assembling these views into a single turntable-style video for evaluation.

For qualitative evaluation, we use a collection of real-world videos sourced from the internet, the DAVIS dataset [Pont-Tuset et al. 2017], and from BANMo [Yang et al. 2022]. These clips are captured in casual, in-the-wild environments, exhibiting diverse and complex camera and object motions. Each video ranges from 40 to 300 frames in length, providing rich temporal dynamics for assessment.

### 4.2 Implementation Details

We train the pose estimation network for 4,000 iterations using the Adam optimizer with a learning rate of  $5 \times 10^{-4}$ ,  $\beta_1 = 0.9$ ,  $\beta_2 = 0.999$ . We train the deformation model for 2,000 iterations using the AdamW optimizer with  $\beta_1 = 0.9$  and  $\beta_2 = 0.99$  for the reference view reconstruction stage. The Posenet training takes 1 hour, and the optimization of the deformation model takes 1.5 hours on a single NVIDIA A6000 GPU.

### 4.3 Baselines

We compare PAD3R with video-to-4D reconstruction methods, including STAG4D [Zeng et al. 2024], L4GM [Ren et al. 2024], DreamMesh4D (DM4D) [Li et al. 2024] and BANMo [Yang et al. 2022]. STAG4D, L4GM and DreamMesh4D do not account for dynamic camera motion, operating under the assumption of a static camera.

### 4.4 Quantitative Results

We follow the evaluation protocol from Consistent4D [Jiang et al. 2024], reporting on perceptual similarity using LPIPS [Zhang et al. 2018], CLIP [Radford et al. 2021] for image similarity, and FVD [Unterthiner et al. 2018] metric to assess video temporal coherence between the ground truth and rendered novel view images. Results are summarized in Table 1. Under the static camera setting, PAD3R outperforms prior approaches, including STAG4D [Zeng et al. 2024], DreamMesh4D [Li et al. 2024], and L4GM [Ren et al. 2024], achieving the best scores across all metrics. Furthermore, in a dynamic camera setting (i.e., where we estimate the camera poses by assuming they are unknown), our method remains competitive, surpassing

**Table 1. Quantitative Results on Consistent4D Dataset.** Consistent4D Dataset includes videos captured from a single viewpoint and is evaluated across four novel views. The training schemes of STAG4D [Zeng et al. 2024] and DreamMesh4D (DM4D) [Ren et al. 2024] align with data that lacks camera or scene motion, which contrasts with our method’s capability to model dynamic camera movements. For this evaluation dataset, PAD3R achieves comparable results against STAG4D [Zeng et al. 2024] and DreamMesh4D [Ren et al. 2024] and outperforms BANMo [Yang et al. 2022] that model camera dynamics. █: best, █: second-best, █: third-best.

Methods	Camera modeling	LPIPS ↓	FVD ↓	CLIP ↑
STAG4D [Zeng et al. 2024]	✗	0.134	1015.57	0.917
L4GM [Ren et al. 2024]	✗	0.152	874.49	0.921
DM4D [Li et al. 2024]	✗	0.128	688.84	0.936
BANMo [Yang et al. 2022]	✓	0.279	1587.10	0.808
PAD3R (w/ static camera)	✗	0.126	613.73	0.941
PAD3R	✓	0.137	645.09	0.942

**Table 2. Quantitative Results on Artemis Dataset.** The Artemis Dataset consists of rendered turntable videos of synthetic animals covering different angles of 40 degrees and 140 degrees. PAD3R achieves the best result, as methods like STAG4D [Zeng et al. 2024], L4GM [Ren et al. 2024], and DreamMesh4D (DM4D) [Li et al. 2024] were unable to handle large camera motion with a static camera assumption. <sup>†</sup> Note that we split the input videos into chunks for L4GM due to limited vram. █: best, █: second-best, █: third-best

Methods	Camera modeling	LPIPS ↓	FVD ↓	CLIP ↑
STAG4D [Zeng et al. 2024]	✗	0.240	1512.97	0.862
L4GM <sup>†</sup> [Ren et al. 2024]	✗	0.235	1397.53	0.888
DM4D [Li et al. 2024]	✗	0.232	3020.65	0.904
BANMo [Yang et al. 2022]	✓	0.265	1682.29	0.837
PAD3R (w/ static camera)	✗	0.257	1473.05	0.909
PAD3R	✓	0.184	1060.04	0.930

BANMo [Yang et al. 2022], which also explicitly models camera motion.

For the Artemis benchmark, we select camera views spanning various viewing angles around each object and compile them into turntable video sequences of 20 to 300 frames. Evaluation is conducted using 3 novel views per sequence, each with corresponding ground truth data for quantitative comparison.

We follow the same evaluation protocol as in Consistent4D [Jiang et al. 2024], reporting LPIPS, CLIP and FVD to assess perceptual quality and temporal coherence of the novel views. Quantitative results are presented in Table 2. PAD3R achieves state-of-the-art performance across all metrics, outperforming prior approaches. These results demonstrate the effectiveness of our model in accurately capturing both camera motion trajectories and the complex non-rigid dynamics of objects.

To further assess PAD3R’s capacity to capture camera movements, we analyze how input view coverage affects reconstruction quality. Specifically, we evaluate on five input sequences, each providing

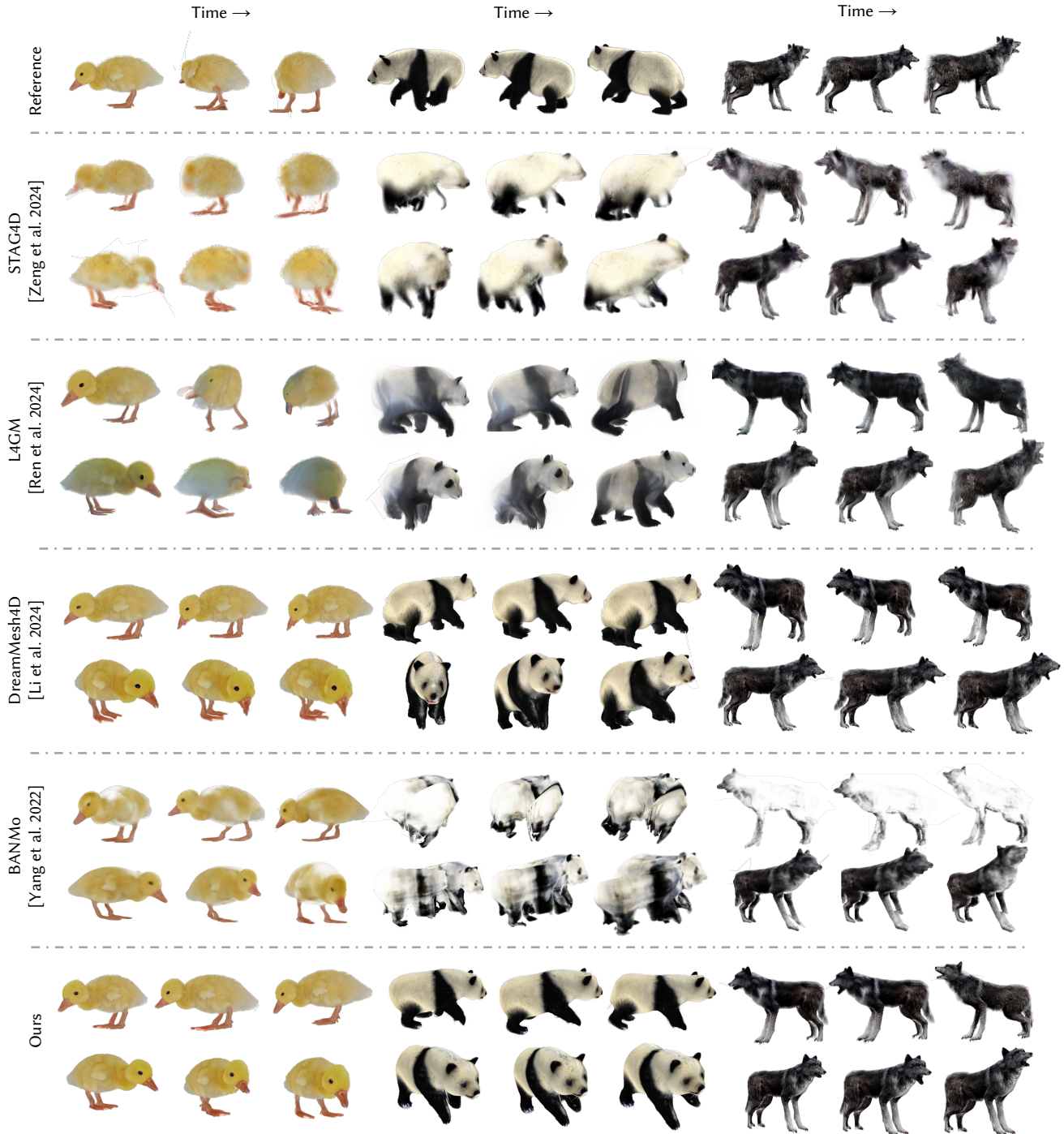


Fig. 5. Comparison of our method against baseline methods on the Artemis dataset. Our method can generate novel views of better quality while remaining faithful to the reference views. DreamMesh4D [Li et al. 2024] suffers from distortions in the mouth and chest regions for the duck sequence, and has the wrong leg geometry for the panda sequence, while our reconstructions do not suffer from those problems. Images sourced from Artemis (©Luo et al., 2022).

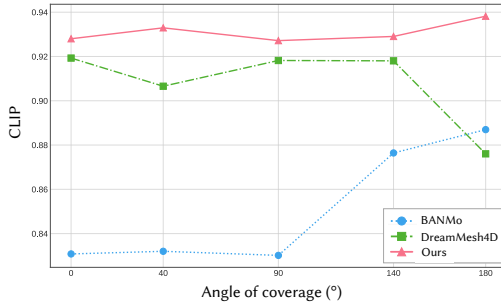


Fig. 6. **Reconstruction quality v.s. input view coverage.** PAD3R consistently achieves high performance across different amounts of view coverage. In contrast, DreamMesh4D [Li et al. 2024] degrades under large camera motion, while BANMo [Yang et al. 2022] performs better with broader view coverage but struggles in limited view cases.

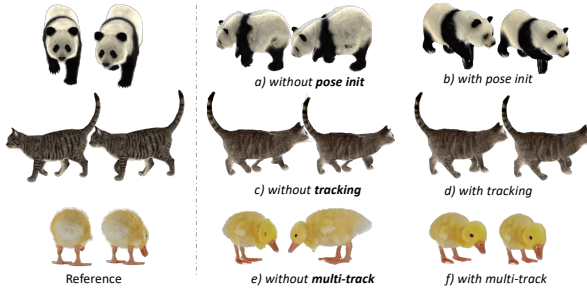


Fig. 7. **Ablation.** We show the contributions of each of our components: a) without pose initialization vs b) with pose initialization, c) without tracking vs d) with tracking regularization, and e) without multi-tracking vs f) with multi-tracking regularization. We observe that without pose initialization in (a), there is a degradation in the panda’s geometry and wrong orientation. Without tracking in (c), the reconstructed cat has an extra front leg. For (e), the orientation of the duck is wrong. Images sourced from Artemis (©Luo et al., 2022).

a different extent of viewpoint variation, 0°(single-view), 40°, 90°, 140° and 180°. Figure 6 shows the reconstruction performance against input view coverage of our method against the baseline method DreamMesh4D [Li et al. 2024], the current state-of-the-art method that assumes a static camera, and BANMo [Yang et al. 2022], which explicitly models camera motion.

As illustrated in Figure 6, PAD3R maintains consistently high reconstruction quality across varying view coverage angles. In contrast, due to its static camera assumption, DreamMesh4D exhibits a steady decline in performance as the range of viewpoints expands. Conversely, BANMo [Yang et al. 2022] shows improved results with broader view coverage, but performs poorly under single-view or narrow-view settings. These results underscore the robustness and adaptability of our approach in handling both constrained and dynamic camera motions, enabling accurate reconstructions under diverse conditions.

Table 3. **Ablation results on the Artemis dataset removing each component.**  $cam$  stands for dynamic camera modeling.  $\mathcal{P}_{init}$  stands for initiating camera pose from PoseNet prediction. ■: best, □: second-best, △: third-best.

Method	LPIPS ↓	FVD ↓	CLIP↑
cam	0.198	1022.39	0.916
cam + $\mathcal{P}_{init}$	0.186	1048.95	0.927
cam + $\mathcal{P}_{init}$ + $\mathcal{L}_{track}$	0.181	1015.07	0.926
full method (w. $\mathcal{L}_{multi-track}$ )	0.173	1011.45	0.928

#### 4.5 Qualitative Results

We showcase qualitative results comparing our method against several baseline approaches, including STAG4D [Zeng et al. 2024], DreamMesh4D [Li et al. 2024], L4GM [Ren et al. 2024], and BANMo [Yang et al. 2022]. These evaluations span both controlled synthetic scenes from the Artemis dataset [Luo et al. 2022] and casually captured, in-the-wild videos.

Figure 5 showcases qualitative comparisons on the Artemis dataset [Luo et al. 2022], illustrating PAD3R’s ability to recover high-fidelity textures and accurate geometry under complex object and camera motions. In Figure 8, we extend the evaluation to real-world scenarios. Our method generalizes well to real-world videos, delivering complete, coherent, and stable 3D reconstructions across diverse motions. The supplementary material includes additional results and dynamic visualizations showcasing reconstructions and novel view renderings.

#### 4.6 Ablation Studies

We conduct an ablation study to evaluate the impact of core components in our method: object-centric camera modeling, PoseNet-based pose initialization, and the two proposed tracking objectives:  $\mathcal{L}_{track}$  and  $\mathcal{L}_{multi-track}$ . Quantitative results are reported in Table 3, and qualitative comparisons are shown in Figure 7. We select our final model configuration based on the best overall performance across metrics.

The ablation demonstrates that all components are critical in achieving accurate and detailed 4D reconstruction. PoseNet initialization enhances camera pose estimation, resulting in improved reconstruction. The  $\mathcal{L}_{track}$  loss captures fine-grained motion, particularly around articulated limbs. Incorporating  $\mathcal{L}_{multi-track}$  further boosts temporal consistency by aligning object and camera dynamics. Together, these elements significantly improve both quantitative performance and visual fidelity.

**Impact of Pose Initialization.** We further conduct experiments comparing our personalized PoseNet against state-of-the-art camera pose estimators, MegaSaM [Li et al. 2025] and VGGT [Wang et al. 2025a], to evaluate the effect of initialization quality. As reported in Table 4, using PoseNet predictions consistently achieves the best reconstruction quality without camera refinement. In contrast, off-the-shelf models struggle to estimate accurate object-centric poses due to the lack of static correspondences, leading to degraded reconstruction. Even after enabling camera refinement, our model still achieves the strongest performance when initialized with PoseNet.

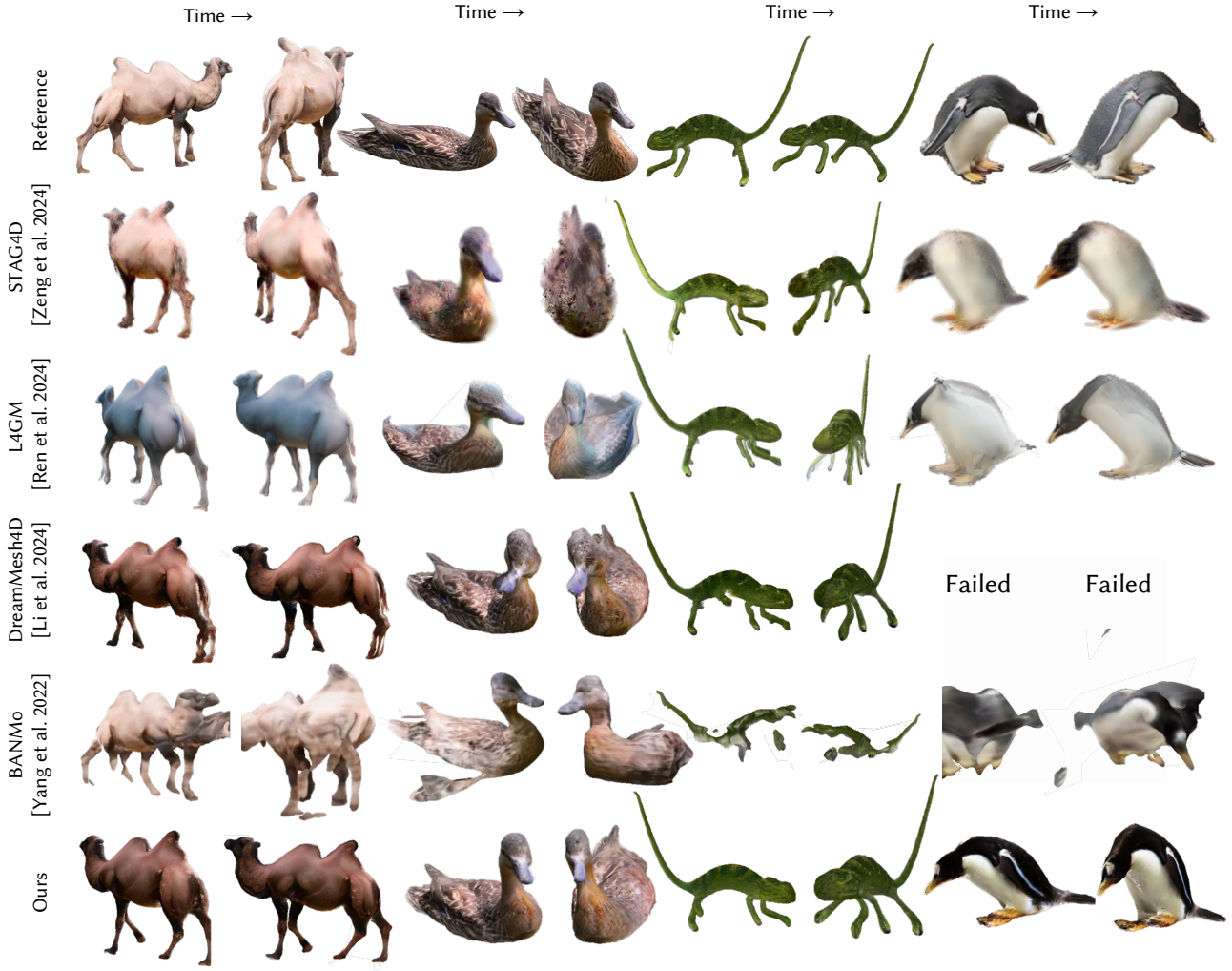


Fig. 8. Qualitative comparison against baseline methods on challenging in-the-wild videos with large camera and object root body motion. Ours is able to achieve consistently high-quality reconstruction while baseline methods fail. Images sourced from DAVIS (©DAVIS Challenge organizers) and ©Pexels.

Table 4. Ablation results with off-the-shelf camera pose estimators.

We compare our personalized PoseNet against state-of-the-art methods MegaSaM [Li et al. 2025] and VGGT [Wang et al. 2025a] on the Artemis dataset, evaluating reconstruction quality with and without camera refinement. Our PoseNet consistently achieves the best performance across all metrics. ■: best, □: second-best.

Methods	Camera modeling	LPIPS ↓	FVD ↓	CLIP ↑
MegaSaM [Li et al. 2025]	✗	0.214	1781.95	0.710
VGGT [Wang et al. 2025a]	✗	0.210	1753.32	0.729
PAD3R (PoseNet)	✗	0.190	1180.52	0.897
MegaSaM [Li et al. 2025]	✓	0.194	1094.42	0.833
VGGT [Wang et al. 2025a]	✓	0.174	1026.94	0.928
PAD3R (PoseNet)	✓	0.173	1011.45	0.928

The experiments demonstrate the importance of reliable object-centric pose estimation. These results underscore the need for personalized pose estimation to achieve robust and temporally coherent 4D reconstruction.

#### 4.7 Limitations

While PAD3R has demonstrated improved performance over the state-of-the-art on dynamic 3D object reconstruction from videos, it has several limitations. First, since our method employs per-video optimization, it is not suitable for applications that require real-time or rapid processing. Second, while off-the-shelf image-to-3D models have shown great progress, they sometimes produce erroneous 3D shapes and overly smooth textures. This, in turn, may adversely affect the training of the pose estimation model. This can be potentially mitigated by jointly learning the canonical 3D shape and appearance model (together with camera poses and deformation)



Fig. 9. Composing our object-level 4D reconstructions (left) with static background Gaussians produces a full dynamic scene reconstruction (right). Images sourced from DAVIS (©DAVIS Challenge organizers) and ©Pexels.

directly from the video. However, our initial attempts found it challenging due to the ambiguity. Third, the 2D tracking models may be inaccurate, particularly when rapid motion or heavy occlusion occurs. Also, no constraints can be derived from unseen viewpoints. To address this, we believe that using motion priors (e.g., from video diffusion models) is a promising future direction.

## 5 Conclusion

In this work, we present PAD3R for reconstructing dynamic, articulated objects from casually captured monocular videos. We address the limitations of both optimization-based methods and recent learning-based approaches. We achieve high-fidelity reconstructions that preserve geometric and texture integrity by leveraging an instance-specific pose estimator, a generative prior, and a novel multi-tracking regularization. Our evaluation of the Artemis video dataset highlights the improvements of our method over existing baselines, particularly in handling videos with large camera and object root-body motion. Our work provides a robust and flexible framework for extracting dynamic 3D representations from casual videos, thereby broadening the applicability of 4D reconstruction techniques to various real-world scenarios.

**Acknowledgments.** We sincerely appreciate Shunsuke Saito for his early explorations with us, insightful discussions, and generous support.

## References

Ang Cao and Justin Johnson. 2023. HexPlane: A Fast Representation for Dynamic Scenes. In *CVPR*.

Matt Deitke, Dustin Schwenk, Jordi Salvador, Luca Weihs, Oscar Michel, Eli Vander-Bilt, Ludwig Schmidt, Kiana Ehsani, Aniruddha Kembhavi, and Ali Farhadi. 2023. Objaverse: A universe of annotated 3d objects. In *CVPR*.

Yuanxing Duan, Fangyin Wei, Qiyu Dai, Yuhang He, Wenzheng Chen, and Baoquan Chen. 2024. 4d-rotor gaussian splatting: towards efficient novel view synthesis for dynamic scenes. In *ACM SIGGRAPH*.

Sara Fridovich-Keil, Giacomo Meanti, Frederik Rahbæk Warburg, Benjamin Recht, and Angjoo Kanazawa. 2023. K-Planes: Explicit Radiance Fields in Space, Time, and Appearance. In *CVPR*.

Chen Gao, Ayush Saraf, Johannes Kopf, and Jia-Bin Huang. 2021. Dynamic View Synthesis from Dynamic Monocular Video. In *ICCV*.

Antoine Guédon and Vincent Lepetit. 2024. SuGaR: Surface-Aligned Gaussian Splatting for Efficient 3D Mesh Reconstruction and High-Quality Mesh Rendering. In *CVPR*.

Jonathan Ho, Ajay Jain, and Pieter Abbeel. 2020. Denoising diffusion probabilistic models. *NeurIPS* (2020).

Yanqin Jiang, Li Zhang, Jin Gao, Weiming Hu, and Yao Yao. 2024. Consistent4D: Consistent 360° Dynamic Object Generation from Monocular Video. In *ICLR*.

Nikita Karaev, Iurii Makarov, Jianyuan Wang, Natalia Neverova, Andrea Vedaldi, and Christian Rupprecht. 2024. CoTracker3: Simpler and Better Point Tracking by Pseudo-Labelling Real Videos. In *arXiv:2410.11831*.

Ladislav Kavan, Steven Collins, Jiví vZára, and Carol O'Sullivan. 2008. Geometric skinning with approximate dual quaternion blending. *TOG* (2008).

Alex Kendall and Yarin Gal. 2017. What uncertainties do we need in bayesian deep learning for computer vision? *Advances in neural information processing systems* 30 (2017).

Bernhard Kerbl, Georgios Kopanas, Thomas Leimkühler, and George Drettakis. 2023. 3d gaussian splatting for real-time radiance field rendering. *ACM TOG* (2023).

Jiahui Lei, Yijia Weng, Adam Harley, Leonidas Guibas, and Kostas Daniilidis. 2024. MoSca: Dynamic Gaussian Fusion from Casual Videos via 4D Motion Scaffolds. *arXiv preprint arXiv:2405.17421* (2024).

Zhiqi Li, Yiming Chen, and Peidong Liu. 2024. DreamMesh4D: Video-to-4D Generation with Sparse-Controlled Gaussian-Mesh Hybrid Representation. In *NeurIPS*.

Zhengqi Li, Richard Tucker, Forrester Cole, Qianqian Wang, Linyi Jin, Vickie Ye, Angjoo Kanazawa, Aleksander Holynski, and Noah Snavely. 2025. MegaSaM: Accurate, Fast and Robust Structure and Motion from Casual Dynamic Videos. In *CVPR*.

Qingming Liu, Yuan Liu, Jiepeng Wang, Xianqiang Lyu, Peng Wang, Wenping Wang, and Junhui Hou. 2025. MoDGS: Dynamic Gaussian Splatting from Casually-captured Monocular Videos with Depth Priors. In *ICLR*.

Ruoshi Liu, Rundi Wu, Basile Van Hoorick, Pavel Tokmakov, Sergey Zakharov, and Carl Vondrick. 2023. Zero-1-to-3: Zero-shot one image to 3d object. In *ICCV*.

Matthew Loper, Naureen Mahmood, Javier Romero, Gerard Pons-Moll, and Michael J. Black. 2015. SMPL: A Skinned Multi-Person Linear Model. *SIGGRAPH Asia* (2015).

Jonathon Luiten, Georgios Kopanas, Bastian Leibe, and Deva Ramanan. 2024. Dynamic 3D Gaussians: Tracking by Persistent Dynamic View Synthesis. In *3DV*.

Haimin Luo, Teng Xu, Yuheng Jiang, Chenglin Zhou, Qiwei Qiu, Yingliang Zhang, Wei Yang, Lan Xu, and Jingyi Yu. 2022. Artemis: Articulated Neural Pets with Appearance and Motion Synthesis. *ACM Trans. Graph.* (2022).

Ben Mildenhall, Pratul P. Srinivasan, Matthew Tancik, Jonathan T. Barron, Ravi Ramamoorthi, and Ren Ng. 2020. NeRF: Representing Scenes as Neural Radiance Fields for View Synthesis. In *ECCV*.

Maxime Oquab, Timothée Darret, Theo Moutakanni, Huy V. Vo, Marc Szafraniec, Vasil Khalidov, Pierre Fernandez, Daniel Haziza, Francisco Massa, Alaaeldin El-Nouby, Russell Howes, Po-Yao Huang, Hu Xu, Vasu Sharma, Shang-Wen Li, Wojciech Galuba, Mike Rabbat, Mido Assran, Nicolas Ballas, Gabriel Synnaeve, Ishan Misra, Hervé Jegou, Julien Mairal, Patrick Labatut, Armand Joulin, and Piotr Bojanowski. 2023. DINOv2: Learning Robust Visual Features without Supervision.

Zijie Pan, Zeyu Yang, Xiatian Zhu, and Li Zhang. 2024. Efficient4D: Fast Dynamic 3D Object Generation from a Single-view Video. *arXiv preprint arXiv 2401.08742* (2024).

Jangho Park, Taesung Kwon, and Jong Chul Ye. 2025. Zero4D: Training-Free 4D Video Generation From Single Video Using Off-the-Shelf Video Diffusion Model. *arXiv preprint arXiv:2503.22622* (2025).

Keunhong Park, Utkarsh Sinha, Jonathan T Barron, Sofien Bouaziz, Dan B Goldman, Steven M Seitz, and Ricardo Martin-Brualla. 2021a. Nerfies: Deformable neural radiance fields. In *ICCV*.

Keunhong Park, Utkarsh Sinha, Peter Hedman, Jonathan T. Barron, Sofien Bouaziz, Dan B Goldman, Ricardo Martin-Brualla, and Steven M. Seitz. 2021b. HyperNeRF: A Higher-Dimensional Representation for Topologically Varying Neural Radiance Fields. *ACM TOG* (2021).

Sang Il Park and Jessica K Hodgins. 2006. Capturing and animating skin deformation in human motion. *TOG* (2006).

Jordi Pont-Tuset, Federico Perazzi, Sergi Caelles, Pablo Arbeláez, Alex Sorkine-Hornung, and Luc Van Gool. 2017. The 2017 davis challenge on video object segmentation. *arXiv preprint arXiv:1704.00675* (2017).

Ben Poole, Ajay Jain, Jonathan T. Barron, and Ben Mildenhall. 2023. DreamFusion: Text-to-3D using 2D Diffusion. *ICLR*.

Albert Pumarola, Enric Corona, Gerard Pons-Moll, and Francesc Moreno-Noguer. 2021. D-nerf: Neural radiance fields for dynamic scenes. In *CVPR*.

Alec Radford, Jong Wook Kim, Chris Hallacy, Aditya Ramesh, Gabriel Goh, Sandhini Agarwal, Girish Sastry, Amanda Askell, Pamela Mishkin, Jack Clark, et al. 2021. Learning transferable visual models from natural language supervision. In *ICML*.

Jiawei Ren, Liang Pan, Jiaxiang Tang, Chi Zhang, Ang Cao, Gang Zeng, and Ziwei Liu. 2023. DreamGaussian4D: Generative 4D Gaussian Splatting. *arXiv preprint arXiv:2312.17142* (2023).

Jiawei Ren, Kevin Xie, Ashkan Mirzaei, Hanxue Liang, Xiaohui Zeng, Karsten Kreis, Ziwei Liu, Antonio Torralba, Sanja Fidler, Seung Wook Kim, and Huan Ling. 2024. L4GM: Large 4D Gaussian Reconstruction Model. In *NeurIPS*.

Jiaming Song, Chenlin Meng, and Stefano Ermon. 2021. Denoising diffusion implicit models. *ICLR* (2021).

Liangchen Song, Anpei Chen, Zhong Li, Zhang Chen, Lele Chen, Junsong Yuan, Yi Xu, and Andreas Geiger. 2023. NeRFPlayer: A Streamable Dynamic Scene Representation with Decomposed Neural Radiance Fields. *IEEE TVCG* (2023).

Olga Sorkin and Marc Alexa. 2007. As-rigid-as-possible surface modeling. In *Proceedings of the Fifth Eurographics Symposium on Geometry Processing* (Barcelona, Spain) (*SGP '07*). Eurographics Association, Goslar, DEU, 109–116.

Colton Stearns, Adam Harley, Mikaela Uy, Florian Dubost, Federico Tombari, Gordon Wetzstein, and Leonidas Guibas. 2024. Dynamic gaussian marbles for novel view synthesis of casual monocular videos. In *SIGGRAPH Asia*.

Robert W. Sumner, Johannes Schmid, and Mark Pauly. 2007. Embedded deformation for shape manipulation. *SIGGRAPH* (2007).

Tao Tu, Ming-Feng Li, Chieh Hubert Lin, Yen-Chi Cheng, Min Sun, and Ming-Hsuan Yang. 2025. Dreamo: Articulated 3d reconstruction from a single casual video. In *WACV*.

Thomas Unterthiner, Sjoerd Van Steenkiste, Karol Kurach, Raphael Marinier, Marcin Michalski, and Sylvain Gelly. 2018. Towards accurate generative models of video: A new metric & challenges. *arXiv preprint arXiv:1812.01717* (2018).

Jianyu Wang, Minghao Chen, Nikita Karaev, Andrea Vedaldi, Christian Rupprecht, and David Novotny. 2025a. VGGT: Visual Geometry Grounded Transformer. In *CVPR*.

Qianqian Wang, Vickie Ye, Hang Gao, Weijia Zeng, Jake Austin, Zhengqi Li, and Angjoo Kanazawa. 2024. Shape of Motion: 4D Reconstruction from a Single Video. *arXiv preprint arXiv:2407.13764* (2024).

Shizun Wang, Xingyi Yang, QiuHong Shen, Zhenxiang Jiang, and Xinchao Wang. 2025b. Gflow: Recovering 4d world from monocular video. In *AAAI*.

Xinzhou Wang, Yikai Wang, Junliang Ye, Zhengyi Wang, Fuchun Sun, Pengkun Liu, Ling Wang, Kai Sun, Xintong Wang, and Bin He. 2023b. AnimatableDreamer: Text-Guided Non-rigid 3D Model Generation and Reconstruction with Canonical Score Distillation. *arXiv preprint arXiv:2312.03795* (2023).

Zhengyi Wang, Cheng Lu, Yikai Wang, Fan Bao, Chongxuan Li, Hang Su, and Jun Zhu. 2023a. ProlificDreamer: High-Fidelity and Diverse Text-to-3D Generation with Variational Score Distillation. *NeurIPS*.

Guanjun Wu, Taoran Yi, Jiemin Fang, Lingxi Xie, Xiaopeng Zhang, Wei Wei, Wenyu Liu, Qi Tian, and Wang Xinggang. 2024. 4D Gaussian Splatting for Real-Time Dynamic Scene Rendering. In *CVPR*.

Rundi Wu, Ruiqi Gao, Ben Poole, Alex Trevithick, Changxi Zheng, Jonathan T. Barron, and Aleksander Holynski. 2025. CAT4D: Create Anything in 4D with Multi-View Video Diffusion Models. In *CVPR*.

Yiming Xie, Chun-Han Yao, Vikram Voleti, Huaizu Jiang, and Varun Jampani. 2024. SV4D: Dynamic 3D Content Generation with Multi-Frame and Multi-View Consistency. *arXiv preprint arXiv:2407.17470* (2024).

Gengshan Yang, Minh Vo, Natalia Neverova, Deva Ramanan, Andrea Vedaldi, and Hanbyul Joo. 2022. BANMo: Building Animatable 3D Neural Models from Many Casual Videos. In *CVPR*.

Ziyi Yang, Xinyu Gao, Wen Zhou, Shaohui Jiao, Yuqing Zhang, and Xiaogang Jin. 2024. Deformable 3d gaussians for high-fidelity monocular dynamic scene reconstruction. In *CVPR*.

Zeyu Yang, Hongye Yang, Zijie Pan, and Li Zhang. 2023. Real-time photorealistic dynamic scene representation and rendering with 4d gaussian splatting. In *ICLR*.

Taoran Yi, Jiemin Fang, Junjie Wang, Guanjun Wu, Lingxi Xie, Xiaopeng Zhang, Wenyu Liu, Qi Tian, and Xinggang Wang. 2024. GaussianDreamer: Fast Generation from Text to 3D Gaussians by Bridging 2D and 3D Diffusion Models. In *CVPR*.

Yuyang Yin, Dejia Xu, Zhangyang Wang, Yao Zhao, and Yunchao Wei. 2023. 4DGen: Grounded 4D Content Generation with Spatial-temporal Consistency. *arXiv preprint arXiv:2312.17225* (2023).

Raza Yunus, Jan Eric Lenssen, Michael Niemeyer, Yiyi Liao, Christian Rupprecht, Christian Theobalt, Gerard Pons-Moll, Jia-Bin Huang, Vladislav Golyanik, and Eddy Ilg. 2024. Recent Trends in 3D Reconstruction of General Non-Rigid Scenes. In *Computer Graphics Forum*.

Yifei Zeng, Yanqin Jiang, Siyu Zhu, Yuanxun Lu, Youtian Lin, Hao Zhu, Weiming Hu, Xun Cao, and Yao Yao. 2024. Stag4d: Spatial-temporal anchored generative 4d gaussians. In *ECCV*.

Richard Zhang, Phillip Isola, Alexei A Efros, Eli Shechtman, and Oliver Wang. 2018. The Unreasonable Effectiveness of Deep Features as a Perceptual Metric. In *CVPR*.

Tingyang Zhang, Qingzhe Gao, Weiyu Li, Libin Liu, and Baoquan Chen. 2024. BAGS: Building Animatable Gaussian Splatting from a Monocular Video with Diffusion Priors. *arXiv preprint arXiv:2403.11427* (2024).

Yuyang Zhao, Zhiwen Yan, Enze Xie, Lanqing Hong, Zhenguo Li, and Gim Hee Lee. 2023. Animate124: Animating One Image to 4D Dynamic Scene. *arXiv preprint arXiv:2311.14603* (2023).